Title

TECHNIQUES USED IN SHIELDING CALCULATIONS FOR HIGH-ENERGY ACCELERATORS: APPLICATIONS TO SPACE SHIELDING

Authors

Wallace, Roger
Sondhaus, Charles.

Publication Date

1962-10-11

UCRL-10439
c.2

University of California

Ernest O. Lawrence Radiation Laboratory

TECHNIQUES USED IN SHIELDING CALCULATIONS FOR HIGH-ENERGY ACCELERATORS: APPLICATIONS TO SPACE SHIELDING

Roger Wallace and Charles Sondhaus

October 11, 1962

Berkeley, California

DISCLAIMER

Symposium on Protection Against Radiation Hazards in Space - Gatlinburg, Tenn., Nov. 1962

UCRL-10439

UNIVERSITY OF CALIFORNIA

Lawrence Radiation Laboratory
Berkeley, California

Contract No. W-7405-eng-48

TECHNIQUES USED IN SHIELDING CALCULATIONS FOR HIGH-ENERGY ACCELERATORS: APPLICATIONS TO SPACE SHIELDING

Roger Wallace and Charles Sondhaus

October 11, 1962

TECHNIQUES USED IN SHIELDING CALCULATIONS FOR HIGH-ENERGY ACCELERATORS: APPLICATIONS TO SPACE SHIELDING*

Roger Wallace and Charles Sondhaus

Lawrence Radiation Laboratory
University of California
Berkeley, California

Abstract

The prediction for the secondary neutron spectrum produced inside of a thick shield is described. The multiplicity of cascade and evaporation secondaries as well as subsequent moderation of the secondary spectrum is described quantitatively. Experimental thick-target neutron yields, as well as Monte Carlo cascade data, are the basis for these estimates.

Introduction

The principle differences between shielding a man in space and shielding the crew of a large accelerator are that the tolerance levels for the space ship are higher, and the integrated incident dose is lower. This reduces the thickness of shield in the space ship relative to that in the accelerator. The detailed investigation of this difference is not the subject of this paper. We only attempt to show how approximate estimates for the shielding of accelerators can be made. These methods and the data used in them are applicable to the space-ship problem.

The spectrum of protons incident on a space ship is both continuous and somewhat softer than the monoenergetic protons that would emerge from a high-energy accelerator in the several-hundred-MeV region. This difference tends to reduce greatly the number of secondary neutrons produced and emphasizes the role of primary protons that may actually penetrate the space-ship wall. Such wall penetration by protons is not characteristic of accelerator-shield situations. The companion paper by Sondhaus and Wallace[1] describes the penetration of a thick shield by protons, whereas this paper is largely limited to neutron considerations. For high-energy accelerators it has been found that the gamma-ray dose outside of a very thick shield is only a modest fraction of the neutron dose. This conclusion may not be true in the case of space shielding where the shield may be somewhat thinner and the gamma-ray dose a more important fraction of the neutron dose.

*Work done under the auspices of the U. S. Atomic Energy Commission, and the Joint Atomic Energy Commission--NASA Space Radiation Program.

The technique generally used to estimate shielding is that developed by B. J. Moyer.[2a, 3, 4] While each proton produces a variety of particles as it undergoes collision in the shield, only the neutrons are of biological significance. For protons striking an extended thick target, the total neutron production as a function of energy for carbon, aluminum, copper, and lead is shown in Fig. 1. This total neutron production consists of two parts: "cascade" and "evaporation" neutrons. There are also cascade protons. The cascade particles that are knocked out during the immediate passage of the incident proton by direct interactions between the proton and the individual nucleons in a target nucleus have been extensively treated by Metropolis.[5] The cascade particles, because of momentum conservation, are strongly concentrated in the forward direction relative to the incident-proton direction. Due to their long mean free paths only those cascade particles having energies above 150 MeV need be considered in shielding. Cascade particles would be rather unimportant as secondaries from protons below 100 MeV.

The remainder of the secondary particles are produced by evaporation from the nucleus after the initial proton passage as a result of the excitation energy that is left behind in the nucleus. The evaporation process gives off neutrons isotropically. There has been some augmentation of these curves to allow for a plural cascade within the target nucleus.

The cascade yields of neutrons and protons resulting from either neutron or proton bombardment are shown in Fig. 2. The synthesis of the resulting secondary neutron spectrum results from three parts:

(1) the cascade neutrons above 20 MeV,

(2) the evaporation-neutron spectrum that is peaked in the few MeV region, and

(3) the resulting thermal spectrum which arises from the degradation of the energy of the other two neutron sources.

This three-part synthesis is a natural division of this otherwise far too complex problem for a simple estimate. Of course, the problem is not too complex for a computer approach. The cascade neutrons above 150 MeV are the only part of the spectrum which must initially be considered in the evaluation of the thickness of the shield. This results from the neutrons of lower energy having attenuation lengths substantially shorter than those above 150 MeV. It is only this penetrating high-energy component that controls the shield thickness, as can be seen in Fig. 3. There is a plateau in the half-value thicknesses of concrete shielding above 150 MeV. The conclusions that one reaches about concrete are also applicable to most other materials (with the exception of hydrogen) on a gram for gram basis. A thick shield made of liquid hydrogen would need special consideration.

There is, of course, a buildup and an establishment of equilibrium in the secondary neutron spectrum in the first few outer layers of the shield. After equilibrium is established in one or two half-value layers, no further change in the shape of the neutron spectrum occurs with depth in the shield, only an attenuation of the entire spectrum as the highest-energy primaries are attenuated.

Cascade Particles

The spectra of cascade particles computed by Metropolis are shown in Fig. 4 for 460 and 1840 MeV incident protons on aluminum. These spectra seem not to differ very much from each other except of course at the highest energies. These spectra are characteristic of somewhat lower energies as well. These spectra, multiplied by the appropriate normalization factors (given in Fig. 7), are shown in the energy region above 50 MeV on Fig. 5 for incident proton energies of 450, 600, and 850 MeV. It is seen that below about 100 MeV the cascade spectra are essentially the same. These spectra have not yet been degraded by passage through hydrogenous material, therefore no thermal peak is present.

The angular distribution of the cascade particles of Metropolis et al.[5] has been augmented by Moyer using data on the angular distribution of the prongs of nuclear-emulsion stars from the Bevatron and from cosmic rays. Such an angular distribution is shown in Fig. 6. The distribution shown is normalized for 6.2-GeV protons on copper; however, the angular distribution is not sensitive to energy. It is hoped that the extremely valuable work of Metropolis et al., which has served as a basis for so many shielding calculations, will soon be augmented by additional Monte Carlo computations from the Oak Ridge Group.

The number of cascade neutrons per incident proton as a function of proton energy for a variety of target materials is given in Fig. 7. It is seen that for the high energies there is a monatonic increase in the number of cascade neutrons with A, whereas for the energy region below 200 MeV the low-A materials actually have a higher neutron production than the high-A materials.

The number of cascade protons per incident proton as a function of proton energy and target A is shown in Fig. 8. These curves bear a resemblance to those for neutron production in Fig. 7 and the same conclusion can be drawn with respect to production in the light elements. It should be noted that in the energy region near 500 MeV the Fig. 8 cascade-proton curves are in the reverse order with the highest proton production coming from the low A's and the lowest proton production coming from the high A's in contrast to the Fig. 7 cascade-neutron case. Above 1000 MeV the low-A curve does cross over the others but the others still remain in the inverted order. This particular fact is of only minor importance to our present problem since cascade protons have a very limited range and it is really the cascade neutrons that one must consider.

After the shielding thickness becomes quite thick, a similar set of curves could be provided giving neutrons per incident neutron and protons per incident neutron as a function of A and energy. These additional curves would only be useful for some specialized accelerator-shielding situations. In the space-vehicle case we do not have a sufficient number of incident neutrons to concern us and the incident proton case is overwhelmingly dominant.

Evaporation Particles

The most important source of neutrons is the evaporation process. Several authors[6-9] have treated the evaporation of nucleons from nuclei that have been excited by very high-energy neutrons or protons. These evaporation neutrons will provide the low-energy end of our spectrum. Nuclear evaporation is somewhat analogous to the evaporation of the liquid on an atomic scale. The resulting particle spectra are obtained by estimating an excitation energy E_1 for the nucleus as a whole. This estimation, due to Moyer,[3] is shown in detail for A from 20 to 220 in Fig. 9. This set of curves gives the "excitation" energy E_1 left behind in a nucleus by a proton or neutron of energy E. This energy is then considered as a thermal kinetic-energy source for eventual evaporation.

The nuclear temperature produced by the deposition of energy E_1 in a nucleus A by an incident neutron or proton is shown in Fig. 10. Note that nuclear temperatures for the light elements have plateaus in the region of several hundred MeV, making the change in temperature in this region with incident proton energy quite small.

The excitation energy is related to the square of an effective nuclear "temperature" by an empirical parameter[6] (A/10); thus we have

$$E_1 = (A/10)\tau^2, \qquad (1)$$

where E_1 is the nuclear excitation in MeV, and A is the atomic weight of the nucleus. This empirical equation is shown in Fig. 11 for four different values of A. It is seen that the light elements have higher nuclear temperatures than heavy elements for a particular excitation energy. Figures 9, 10, and 11 represent a three-dimensional surface in a space whose coordinates are the total nuclear excitation energy, nuclear temperature and bombarding-proton energy.

The evaporation spectrum itself is given by Eq. (2). The E in front of the exponential instead of the usual $E^{1/2}$ which appears in the

$$N(E)dE = (E/\tau^2)e^{-(E/\tau)}dE \qquad (2)$$

Maxwellian energy distribution is necessary to account for the fact that N(E) is a flux density rather than a numerical density.

To estimate the complete spectrum penetrating the shield, it is now necessary to fit this modified Maxwellian low-energy evaporation end of the spectrum to the Metropolis cascade high-energy tail. This transition fit is made after the area under each individual spectrum has been normalized to the estimated total production of each spectrum's particular component (as given in Table I for the case of aluminum or shown for other A's and E's in Figs. 1, 7, and 12). Note that in Table I it is appropriate for the sum of "cascade" and "evaporation" neutrons to not equal the "total" neutrons. The "total" production is per incident particle on a thick target. The "cascade" and "evaporation" production are per inelastic collision at the quoted energy. The sum of these two productions can be either less than or greater than the "total," depending on the ratio of inelastic-collision proton removal to electromagnetic dE/dx proton energy loss. The total neutron production per inelastic collision and the ratio of the evaporation to the cascade process both as a function of energy and A are given in detail in Figs. 13 and 14. The electromagnetic energy loss changes with proton energy, while the inelastic cross sections are quite constant with energy above 100 MeV as seen in Fig. 15. It is seen that for the lightweight elements the number of evaporation neutrons is quite constant at about one neutron per proton over a wide energy range.

More details of this process are available, such as the suppression of the low-energy particles by the Coulomb barrier, as treated by Dostrovsky[6] and Le Couteur.[7] Particles other than neutrons, such as H, H^2, and H^3, as well as multiple-charged particles, such as He^3 and He^4 can also be estimated as given in Figs. 16 through 20. The doubly charged particles have their evaporation spectrum peaks at about twice the energy of the proton spectrum peak for a nucleus of the same excitation. The angular distribution of the particles emitted in connection with nuclear evaporation is of course isotropic. The evaporation particles produced in an internal target have no chance of their own of penetrating the main shield directly, except for the inner one or two mean free paths of the shield. Therefore, evaporation particles are mainly of interest with regard to the radioactivity that they may induce in the accelerator hardware. This problem is probably not of particular importance for space-craft shielding. The evaporation particles are far more important for inducing radioactivity than are the cascade neutrons, since evaporation particles are considerably more numerous and their energy is more favorable for capture. More extensive data is available on evaporation particles.

Attenuation of the Total Spectrum

Generally the fit between the two parts of the spectra as shown in Fig. 5 is done by eye. Greater accuracy is not appropriate to the degree of approximation which we are making. Direct measurements of shield thickness required for a given attenuation factor, using beams of restricted width, have been made for concrete, water, and a few other materials, but probably not for the materials of interest in

space-craft shielding. Light-weight elements, such as contained in concrete, have shielding values very little different for different A's; this value is mainly proportional to the number of grams of shield per cm^2. A thick shield provides neutron attenuation by absorbing, degrading, or deviating the neutrons by nuclear collisions. At the high energies characteristic of cascade particles, elastically scattered particles are so strongly peaked in forwardly directed diffraction patterns that essentially no geometric deviation or energy loss occurs. Thus, as the incident neutron energy is increased from values characteristic of the evaporation region to values associated with the cascade region, the value of the effective removal cross section for neutrons by a shield decreases from the value of the total cross section to the value of the inelastic cross section. This effect is shown in Tables 2, 3, and 4, from Patterson,[2b] as applied to the elements present in concrete. It is seen that $n\sigma_a(cm^{-1})$ is a figure of merit for the efficiency of each element in the concrete. Table 4 emphasizes the importance of the heavier elements as the neutron energy is raised. Several points calculated from these data for concrete, by Patterson, are plotted in Fig. 21 together with several experimental values for energies from 1 MeV to 4.5 GeV. The agreement between the experimental and calculated values is quite good. The same data appeared in CGS units in Fig. 3. These data only apply to thick shields and poor geometry situations. The companion paper presented by C. Sondhaus[1] will outline some deviations from this which are characteristic of somewhat thinner shields where the proton beam may be considered to survive in a geometrical fashion.

The measurements of σ_{total} and $\sigma_{reaction}$ for various nuclei as a function of neutron energy up to 5 GeV are given by Coor et al.[10] and Atkinson et al.[11] and are shown in Lindenbaum[12] (see Fig. 21). This experimental work shows that the attenuation of neutrons in the high-energy region is essentially constant.

Radiation Emerging from the Shield

Now that the spectrum and angular distribution of the neutrons produced in the target and accelerator hardware by the primary protons have been estimated, a secondary calculation can be made of the penetration of the outer shield by these neutrons. This can be done by using similar data for cascade and evaporation particles produced by neutrons, instead of protons as shown in Figs. 2, 9, 10, 12, and 16 through 20, secured from the same sources as that given earlier for incident protons. The evaporation data are the same as those for incident protons, whereas the cascade values are not. As would be expected, the neutrons are more numerous in neutron-induced cascades than in proton-induced cascades, and vice versa for proton-induced cascades. Cascade-produced mesons gradually increase in importance from 500-MeV incident energy on up. They do not become a controlling factor in the energy range considered in space shielding.

The flux of particles present inside the space-ship shield or outside the accelerator shield now consists of (a) directly transmitted primary neutrons of energy > 150 MeV (from the spectra shown in Fig. 5), and (b) evaporation fragments produced by the high-energy neutrons that suffer inelastic collisions in the last layers of the shield. The number of cascade neutrons making evaporation neutrons and protons by inelastic collisions within a last layer of the shield wall of thickness x is

$$N = N_o(e^{x/\lambda} - 1), \tag{3}$$

where x is measured in from the shielded side of the shield, and λ is the mean free path for inelastic collisions of the cascade neutrons. Assume that half of the evaporation neutrons emerge. This is an obvious overestimate of the number of evaporation neutrons but it will to some extent be compensated for by the further multiplication of a fraction of the cascade neutrons in secondary collisions which again increases the number of evaporation neutrons emerging from the shield. Few of the protons produced in the cascade events in the early part of the shield will emerge from the shield, because of range limitations. There will, however, be protons arising from the evaporation processes emerging from the shield.

Considering a final layer of the shield $x = \lambda$, one mean free path thick, and using the spectra shown in Fig. 5 and values of λ shown in Fig. 15 from Lindenbaum,[12] we estimate that in a particular case each cascade neutron produced in the outer shield will be accompanied by 0.6 fast neutrons and 0.3 protons when it emerges from the shield.

There may also be a small flux of thermal neutrons and gamma rays. The gammas come from thermal neutron capture by the H of the shield (if present) and also from nuclear de-excitations associated with evaporation processes. Typically, the numerical value of the thermal neutron flux is only a few times that of the fast neutrons, so the relative dosage from the thermal neutrons is negligible, if we take RBE values into account, in comparison with the fast neutrons. Ionization-chamber measurements of the gamma-ray dosage are typically one-quarter or less than that arising from fast neutrons.

If one wishes to make an estimate of the spectrum of epithermal neutrons that will be produced by moderation of the cascade and evaporation neutrons and will extend below the evaporation peak, the slowing down spectrum can be approximated by assuming that each emission increment $Q(E_1)\Delta E_1$ gives rise to a flux increment with spectrum $1/E - 1/E_1$. Thus, by integration, the slowing down flux has the spectrum

$$\phi(E) = K_1 \int_E^{E_{max}} Q(E_1)\left(\frac{1}{E} - \frac{1}{E_1}\right) dE_1 . \tag{4}$$

This slowing down flux spectrum is joined by continuity of slope of the thermal spectrum,

$$\phi_{th} = K_2 E^{1/2} e^{-(E/kT)}, \tag{5}$$

which are normalized by requiring the integral from zero energy to 1/2 eV to give the value[13]

$$\phi_{th} = 1.25 \frac{Q}{S}, \tag{6}$$

where Q is the total source strength of fast neutrons and S is the surface area over which they are thermalized (in cm^2).

Conclusions

The data that is presently available and pertinent to the shielding of high-energy proton accelerators has been presented. An approximate method for estimating the neutrons produced in the shield and released into the cabin has been outlined. The production curves for heavier secondaries have been given. Data for meson production, although available, are not included. Should the shield consist of liquid hydrogen, some revision of the data would be necessary since the lowest atomic weight included is A = 20 and the production of neutrons in a liquid hydrogen shield arises through different processes. Neither cascade nor evaporation are possible for H. Various modes of meson production accompanied by neutron production are the only sources of neutrons from H. While data for this type of neutron production is available it has not been accumulated and converted to a useful form for shielding purposes. It is probably true however that neutron production from the hydrogen shield would be considerably reduced relative to that from a shield of higher atomic weight. In general, on a weight basis, a hydrogen shield should be considerably more effective than an equal mass per cm^2 of any other type of material; this difference might be a factor of 2. This is probably not enough to dictate the use of liquid hydrogen relative to other shielding materials, unless it happens to be unusually convenient for propulsion and energy storage reasons, since its low density and temperature make its storage very difficult.

References

1. C. Sondhaus and R. Wallace, Solar Proton Exposure Simulation with the 184-Inch Cyclotron, Lawrence Radiation Laboratory Report UCRL-10447, November 1962 (unpublished).

2a. B. J. Moyer, Method of Calculation of the Shielding Enclosure for the Berkeley Bevatron, in First International Symposium on Protection Near Large Accelerators, Saclay, France, January 1962 (to be published).

2b. H. Wade Patterson, The Effect of Shielding on Radiation Produced by the 730-MeV Synchrocyclotron and the 6.3 GeV Proton Synchrotron at the Lawrence Radiation Laboratory (UCRL-10061, January 1962, in First International Symposium on Protection Near Large Accelerators, Saclay, January 1962 (to be published).

3. B. J. Moyer, Data Related to Nuclear Star Production by High-Energy Protons, Lawrence Radiation Laboratory, June 20, 1961 (private communication).

4. B. J. Moyer, Shielding and Radiation Calculations for USNRDL Cyclotron, Lawrence Radiation Laboratory, October 11, 1960 (private communication).

5. N. Metropolis, R. Bivins, M. Storm, A. Turkevich, J. M. Miller, and G. Friedlander, Phys. Rev. 110, (1958) pp. 185 and 204.

6. I. Dostrovsky, P. Robinowitz, and R. Bivins, Phys. Rev. 111, 1659 (1958).

7. K. J. Le Couteur, Proc. Phys. Soc. (London) A63, 259 (1950).

8. Y. Fujimoto and Y. Yamaguchi, Progr. Theoret. Phys. (Kyoto) 4, 468 (1950); ibid., 5, 787.

9. R. W. Deutsch, Phys. Rev. 97, 1110-23 (1955).

10. T. Coor, D. A. Hill, W. F. Hornyak, L. W. Smith, and G. Snow, Phys. Rev. 98, 1369 (1955).

11. J. H. Atkinson, W. N. Hess, V. Perez-Mendez, and R. Wallace, Phys. Rev. 98, 1369 (1955).

12. S. J. Lindenbaum, Shielding of High-Energy Accelerators, in Ann. Rev. Nucl. Sci. 11, 213 (1961).

13. H. W. Patterson and R. Wallace, A Method of Calibrating Slow-Neutron Detectors, Lawrence Radiation Laboratory Report UCRL-8359, July 1958 (unpublished).

Table 1. Secondary cascade and evaporation-particle production, nuclear excitation energy and temperature for aluminum targets in proton beams of three different energies.

Proton energy (MeV)	Total neutron thick target yield (n/p)on Al	No. cascade[a] neutrons per incident proton on Al per inelastic collision	No. cascade[a] protons per incident proton on Al per inelastic collision	Total[a] no. cascade nucleons per incident proton on Al per inelastic collision	Residual[a] nuclear excitation E_1 (MeV)	Residual[a] nuclear temperature τ (MeV)	No. evaporation neutrons per incident neutron or proton per inelastic collision
450	1.3	1.30	1.85	3.15	63	4.3	1.30
600	2.1	1.40	2.05	3.45	72	4.5	1.50
850	3.3	1.55	2.25	3.80	88	4.9	1.60

a. See ref. 3.

Table 2. N atoms/cm^3 for Berkeley concrete ($\times 10^{22}$).

O	4.73
H	1.73
Si	1.57
Ca	0.26
Al	0.17
Fe	0.053
Na	0.028
K	0.028
Mg	0.013

Table 3. Assumed relation between σ_a, the neutron-attenuation cross section, and σ_{tot}, the total neutron cross section

(MeV)	
1	$\sigma_a = 1.00\ \sigma_{tot}$
5	$\sigma_a = 0.65\ \sigma_{tot}$
14	$\sigma_a = 0.055\sigma_{tot}$
$\geqslant 150$	$\sigma_a = 0.50\ \sigma_{tot}$

Table 4. $N\sigma_a(cm^{-1})$ for various elements ($\times 10^{-2}$).

	1 MeV	14 MeV	270 MeV
O	16	4.4	0.89
H	7.8	0.64	0.026
Si	4.7	1.7	0.41
Ca	0.78	0.33	0.10
Al	0.51	0.16	0.05
Fe	0.16	0.045	0.028

Figure Captions

Fig. 1. Measured total neutron yields per proton stopping in a thick target for C, Al, Cu, and Pb, from Moyer.

Fig. 2. Estimated cascade neutrons and protons produced by incident neutrons or protons of energy E_n on nuclei near A = 20 per incident particle per inelastic collision, from Metropolis et al.[5]

Fig. 3. Half-value reduction thickness for high-energy neutrons in ordinary concrete.

Fig. 4. Energy spectra of cascade nucleons emitted from aluminum, from Metropolis et al.[5]

Fig. 5. Cascade and evaporation-neutron emission spectra from 450-, 600-, and 850-MeV protons on aluminum, per incident proton.

Fig. 6. Angular distribution of neutrons, over 150 MeV in energy, from a single collision in Cu by 6.3-GeV protons (normalized to 8 neutrons/proton), from Metropolis et al.[5]

Fig. 7. Number of cascade neutrons per incident proton as a function of proton energy and target A, from Metropolis et al.[5]

Fig. 8. Number of cascade protons per incident proton per inelastic collision as a function of proton energy and target A, from Metropolis et al.[5]

Fig. 9. Average nuclear excitation energy E_1 deposited in nucleus A by an incident neutron or proton of energy E in one inelastic collision.

Fig. 10. Estimated residual nuclear temperature produced in nucleus A after excitation by a neutron or proton of energy E in one inelastic collision, from Metropolis et al.[5]

Fig. 11. Nuclear temperature τ vs nuclear excitation energy E_1 for various A's.

Fig. 12. Estimated number of evaporation neutrons produced per incident neutron or proton of energy E per inelastic collision, from Metropolis et al.

Fig. 13. Average number of evaporation protons per incident proton or neutron on various A's per inelastic collision vs energy of the incident particle, from Metropolis et al.

Fig. 14. Average number of evaporation H^2 per incident proton or neutron on various A's per inelastic collision vs energy of the incident particle, from Metropolis et al.

Fig. 15. Average number of evaporation H^3 per incident proton or neutron on various A's per inelastic collision vs energy of the incident particle, from Metropolis et al.

Fig. 16. Average number of evaporation He^3 per incident proton or neutron on various A's per inelastic collision vs energy of the incident particle, from Metropolis et al.

Fig. 17. Average number of evaporation He^4 per incident proton or neutron on various A's per inelastic collision vs energy of the incident particle, from Metropolis et al.

Fig. 18. Neutron inelastic cross-sections for C, Al, Cu, and Pb vs incident neutron energy, from Lindenbaum.[12]

Fig. 19. Attenuation of neutrons in ordinary concrete. At 90 and 270 MeV, measurements were made at the 184-Inch 340-MeV cyclotron. At 4.5 GeV the measurement was made at the Bevatron.

Fig. 20. Total neutron production per inelastic collision = cascade + evaporation as a function of the incident proton energy.

Fig. 21. Ratio of evaporation neutrons to cascade neutrons per inelastic collision as a function of the incident proton energy.

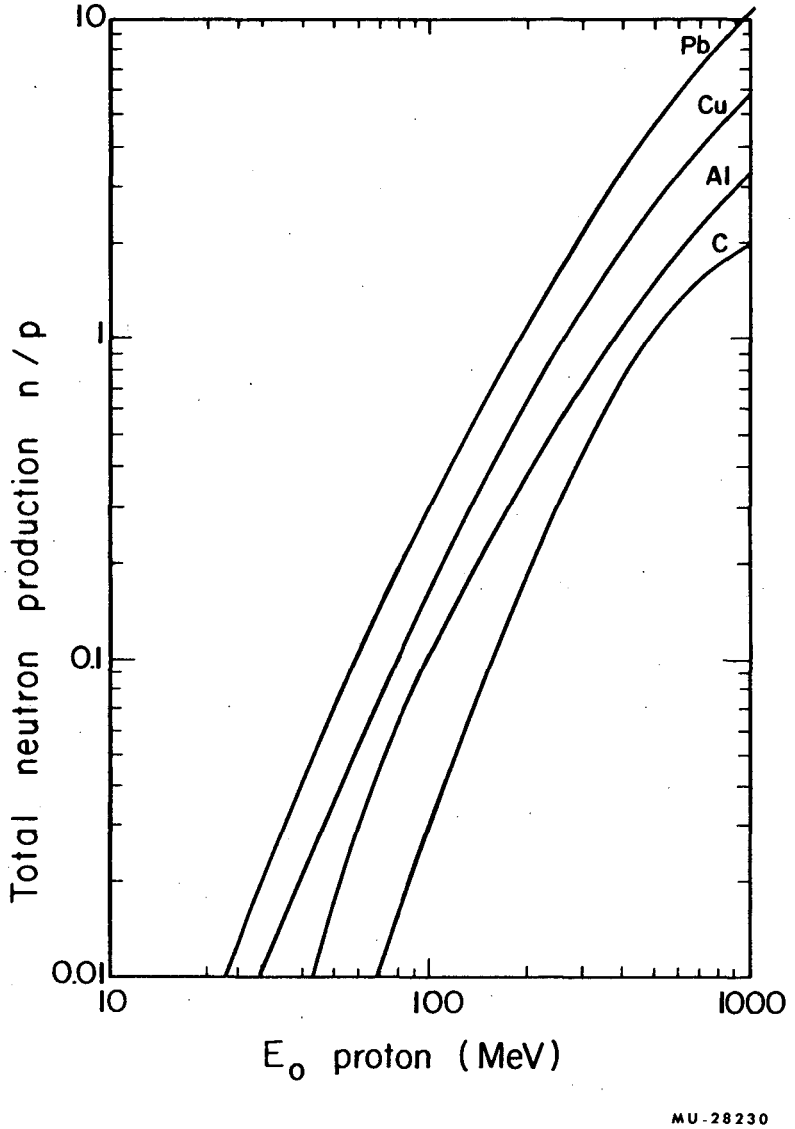
10
1
0.1
0.01
Total neutron production n / p
Pb
Cu
Al
C
10
100
1000
E_o proton (MeV)
MU-28230

Fig. 1.

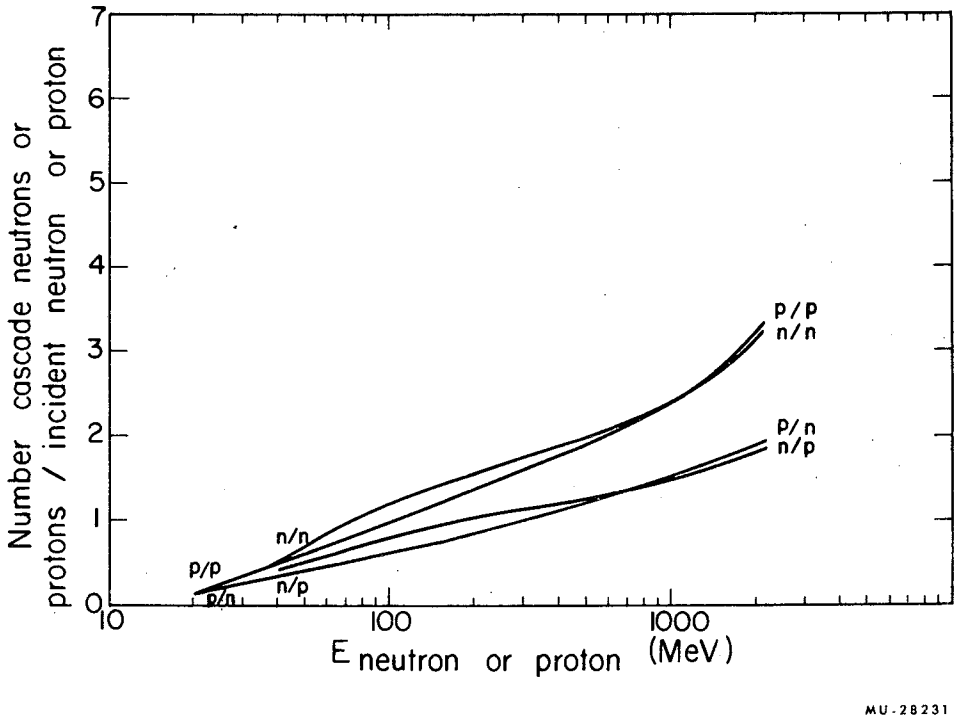
Number cascade neutrons or protons / incident neutron or proton
E neutron or proton (MeV)
p/p
n/n
p/n
n/p
n/n
p/p
p/n
n/p
0
1
2
3
4
5
6
7
10
100
1000
MU-28231

Fig. 2.

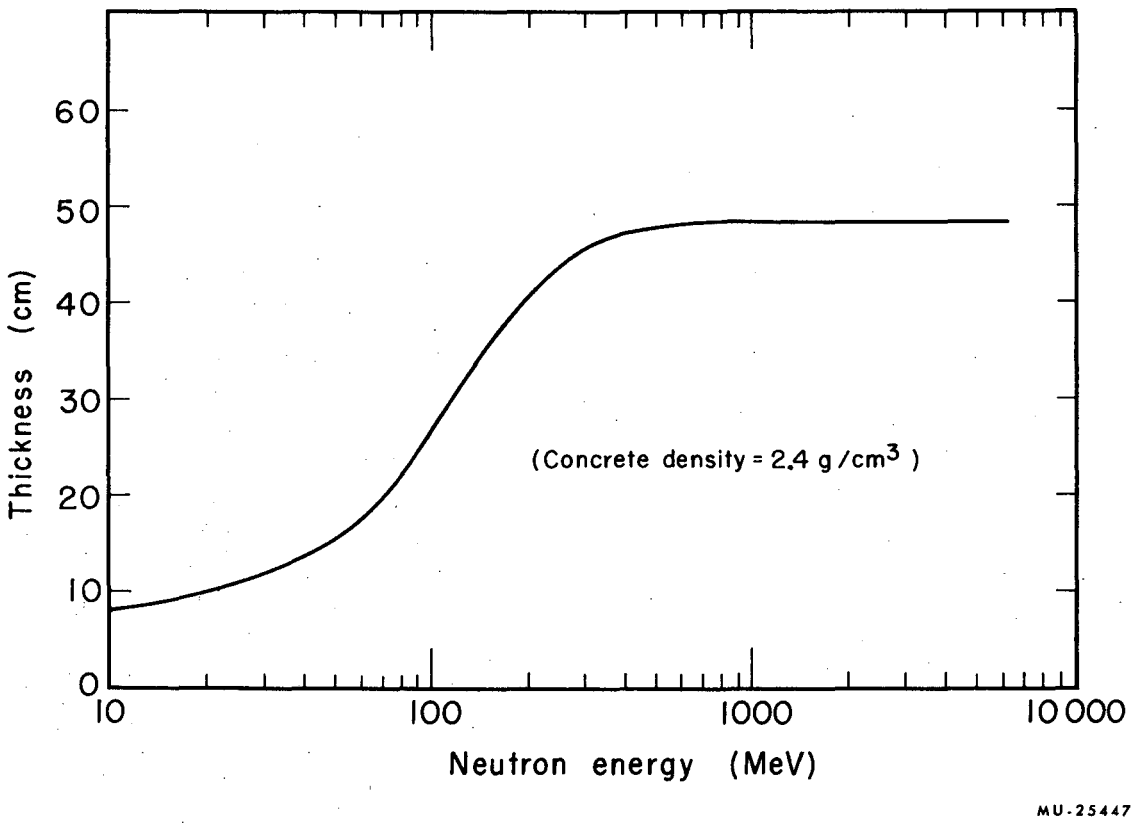
60
50
40
30
20
10
0
Thickness (cm)
(Concrete density = 2.4 g/cm3)
10
100
1000
10 000
Neutron energy (MeV)
MU-25447

Fig. 3.

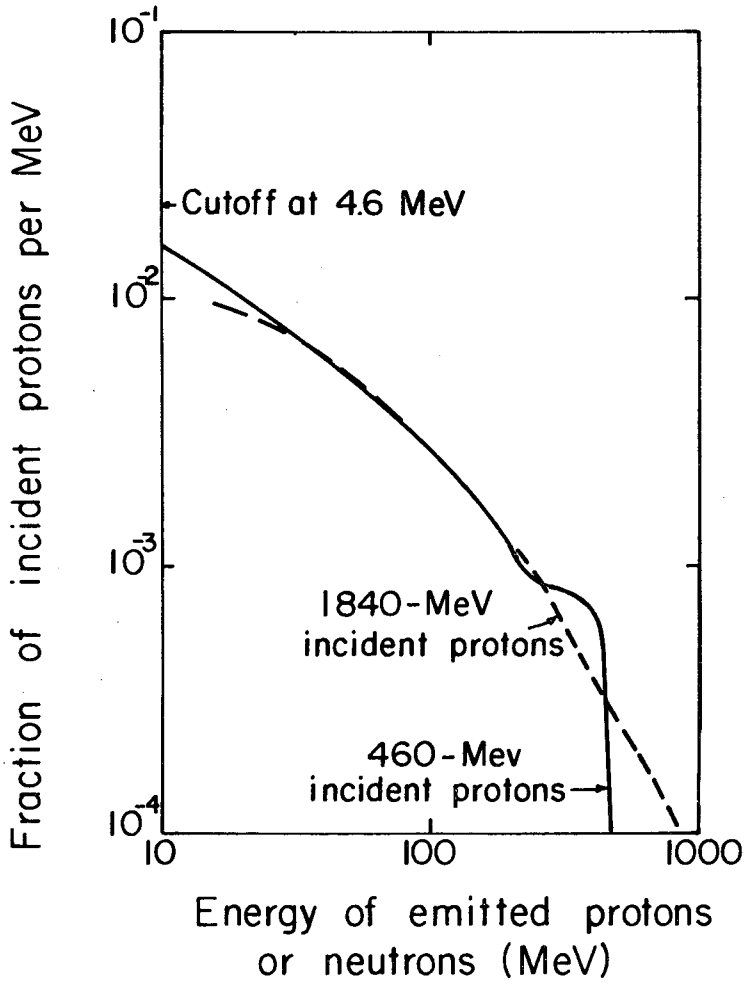
Fraction of incident protons per MeV
10^{-1}
10^{-2}
10^{-3}
10^{-4}
Cutoff at 4.6 MeV
1840-MeV incident protons
460-Mev incident protons
10
100
1000
Energy of emitted protons or neutrons (MeV)
MU-26624

Fig. 4.

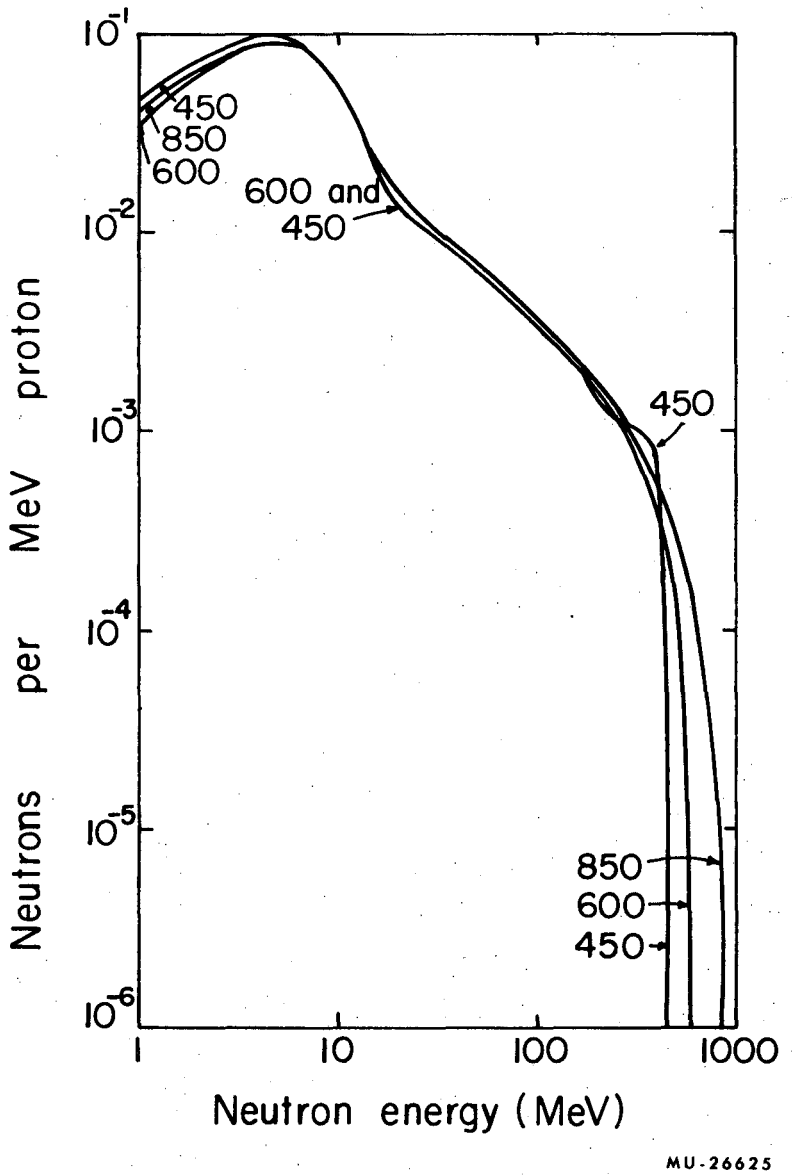
Neutrons per MeV proton
Neutron energy (MeV)
450
850
600
600 and
450
450
850
600
450
MU-26625

Fig. 5.

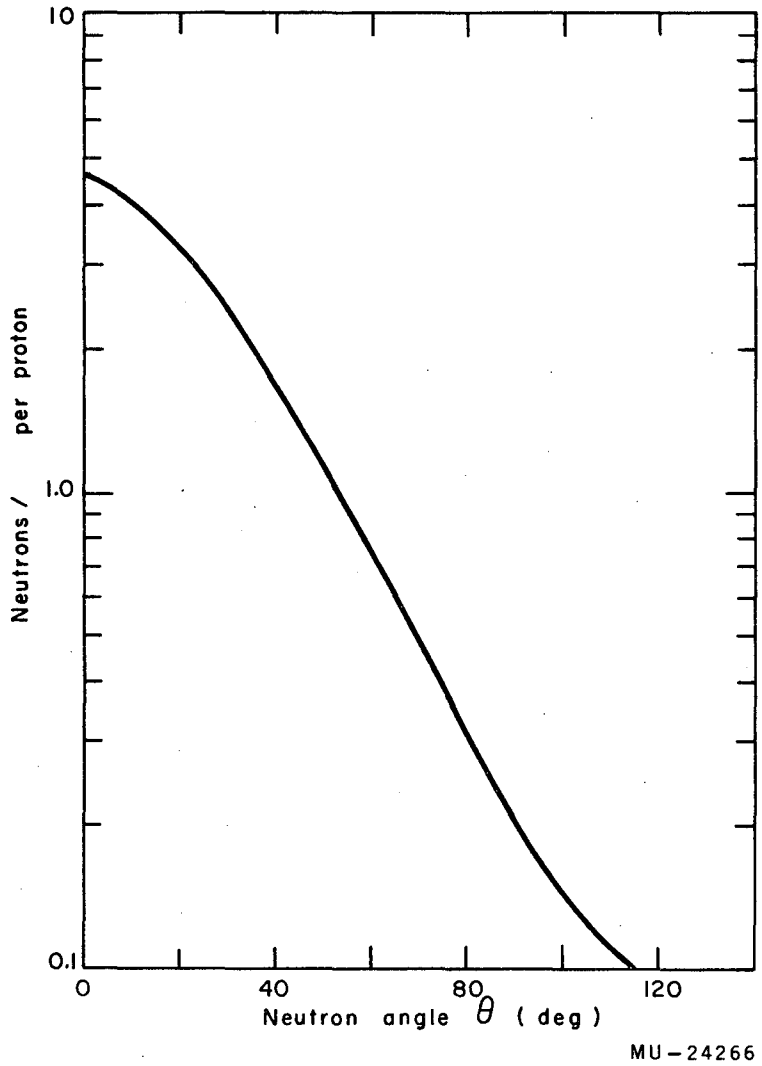
10
1.0
0.1
Neutrons / per proton
0
40
80
120
Neutron angle θ (deg)
MU-24266

Fig. 6.

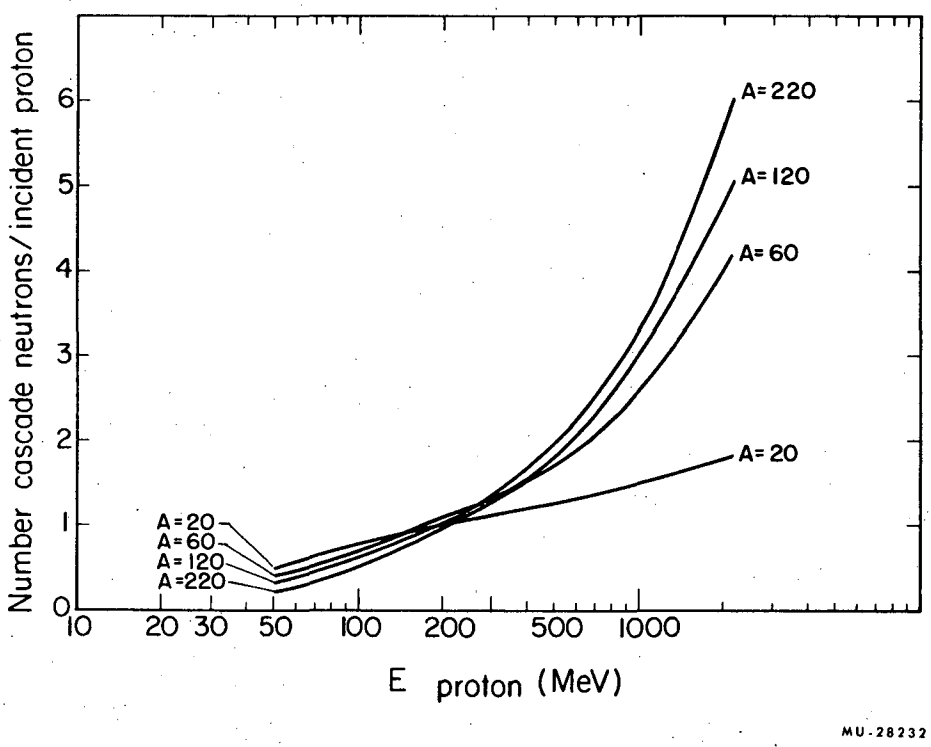
Number cascade neutrons/incident proton
0
1
2
3
4
5
6
10
20
30
50
100
200
500
1000
E proton (MeV)
A=220
A=120
A=60
A=20
A=20
A=60
A=120
A=220
MU-28232

Fig. 7.

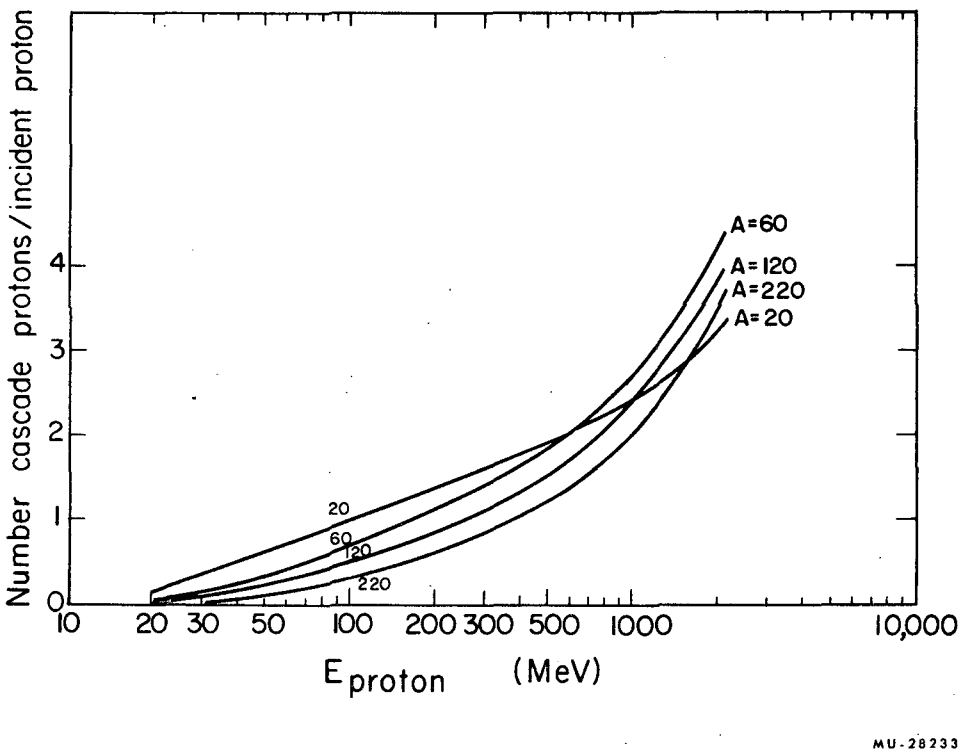
Number cascade protons / incident proton
0
1
2
3
4
10
20
30
50
100
200
300
500
1000
10,000
E proton (MeV)
A=60
A=120
A=220
A=20
20
60
120
220
MU-28233

Fig. 8.

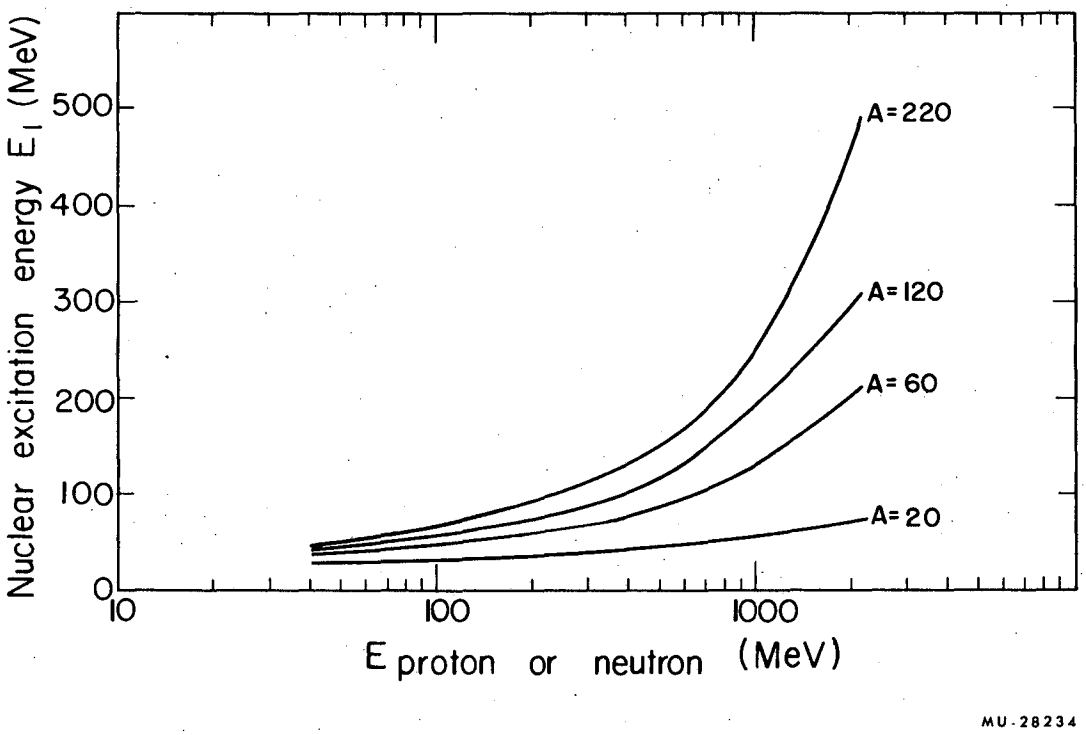
Nuclear excitation energy E_1 (MeV)
500
400
300
200
100
0
10
100
1000
E proton or neutron (MeV)
A=220
A=120
A=60
A=20
MU-28234

Fig. 9.

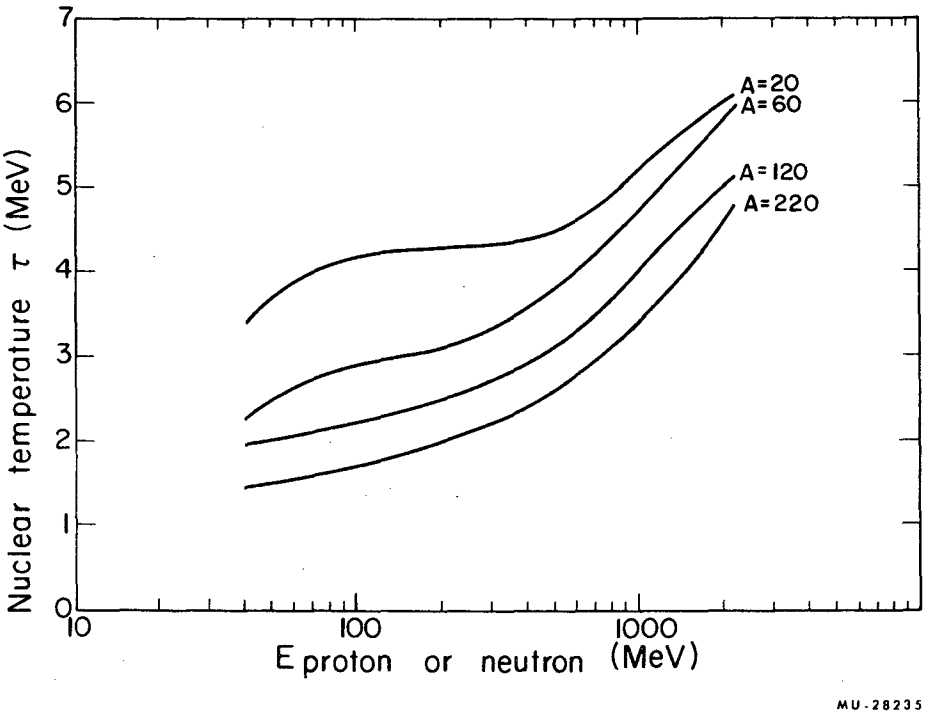
Nuclear temperature τ (MeV)
0
1
2
3
4
5
6
7
10
100
1000
E proton or neutron (MeV)
A=20
A=60
A=120
A=220
MU-28235

Fig. 10.

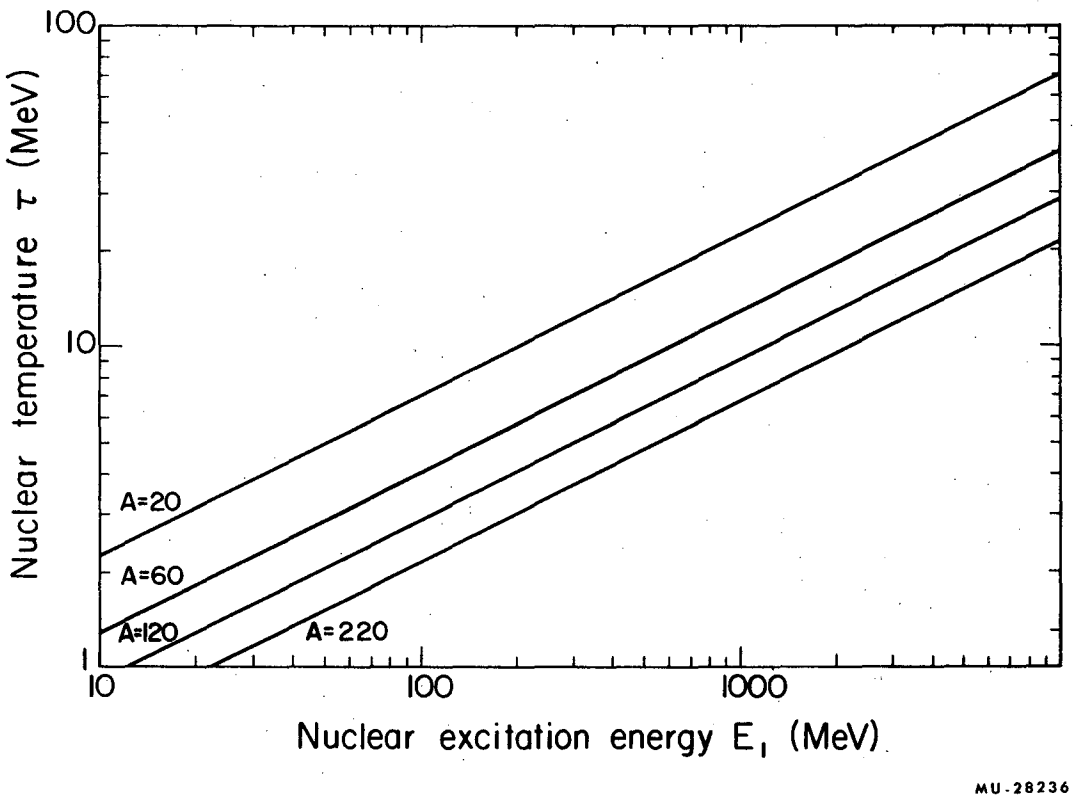
100
10
1
Nuclear temperature τ (MeV)
A=20
A=60
A=120
A=220
10
100
1000
Nuclear excitation energy E, (MeV)
MU-28236

Fig. 11.

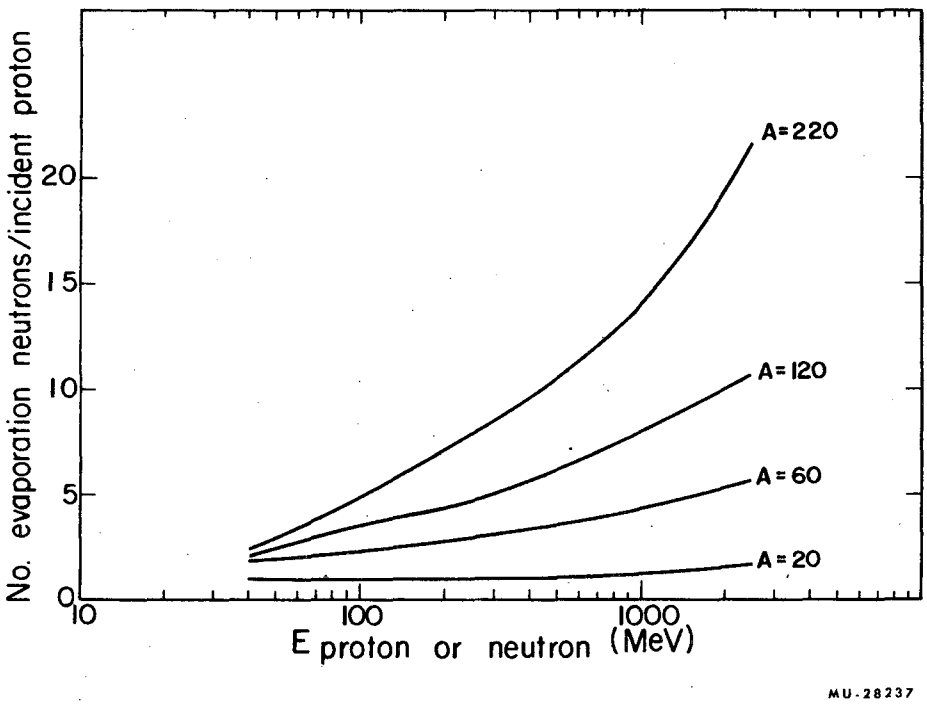
No. evaporation neutrons/incident proton
0
5
10
15
20
10
100
1000
E proton or neutron (MeV)
A=220
A=120
A=60
A=20
MU-28237

Fig. 12.

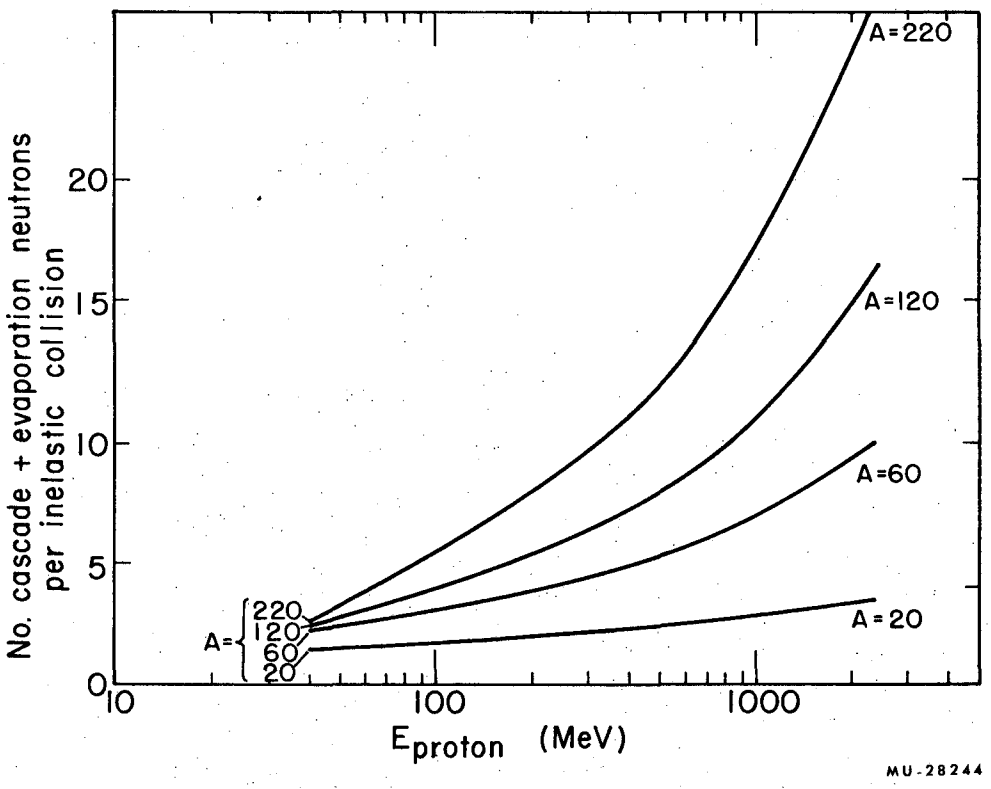
No. cascade + evaporation neutrons per inelastic collision
0
5
10
15
20
10
100
1000
E proton (MeV)
A=220
A=120
A=60
A=20
A=
220
120
60
20
MU-28244

Fig. 13.

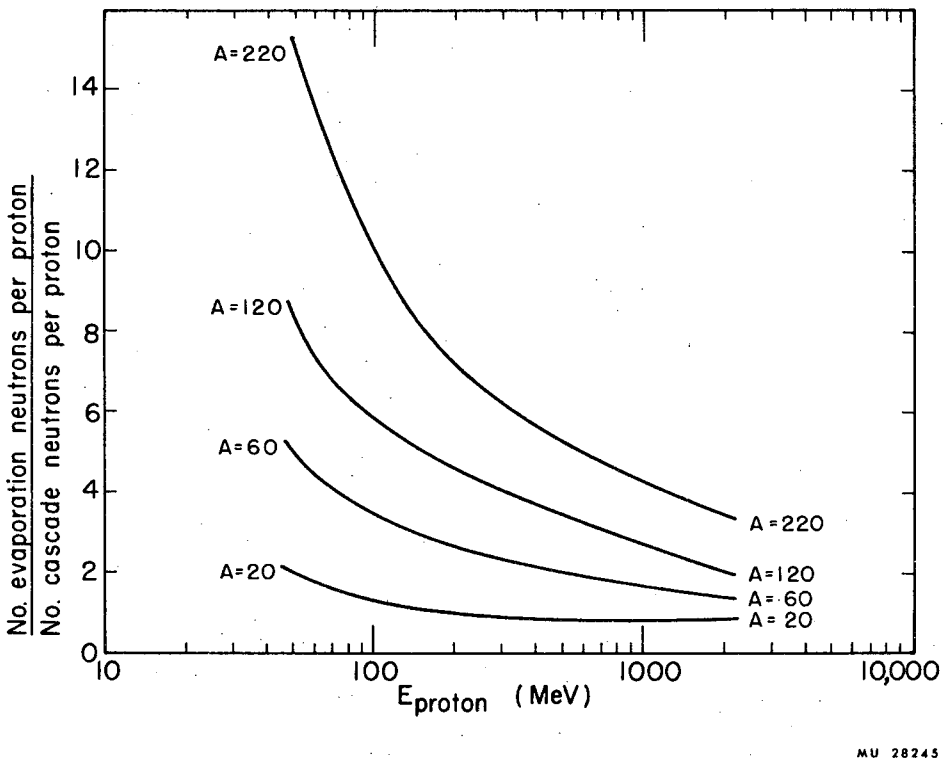
A=220
A=120
A=60
A=20
A=220
A=120
A=60
A=20
14
12
10
8
6
4
2
0
10
100
1000
10,000
E proton (MeV)
No. evaporation neutrons per proton
No. cascade neutrons per proton
MU 28245

Fig. 14.

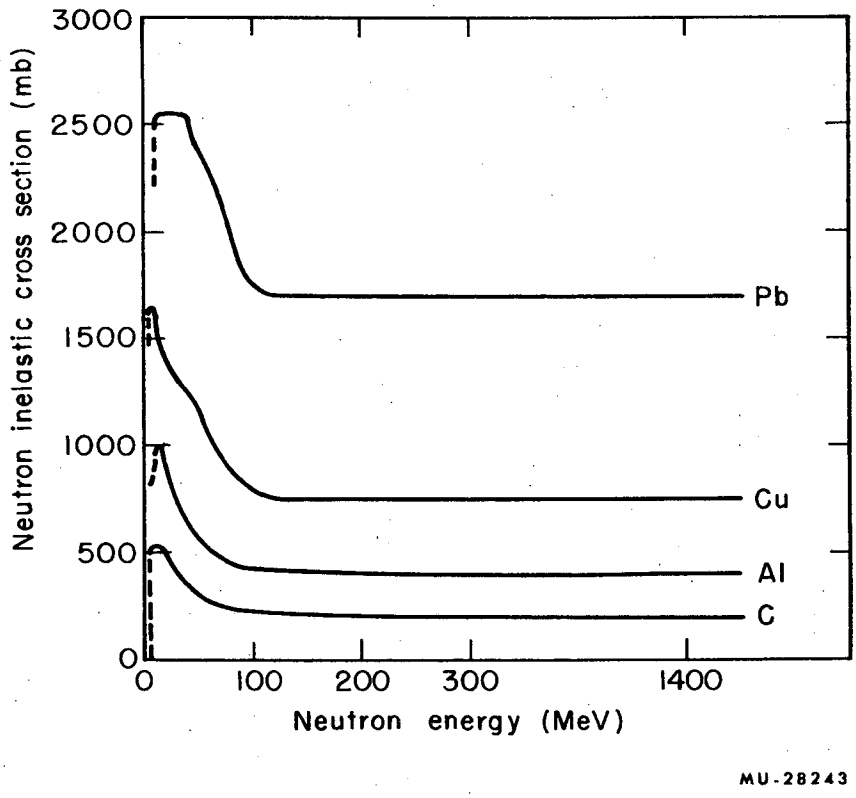
Neutron inelastic cross section (mb)
3000
2500
2000
1500
1000
500
0
0
100
200
300
1400
Neutron energy (MeV)
Pb
Cu
Al
C
MU-28243

Fig. 15.

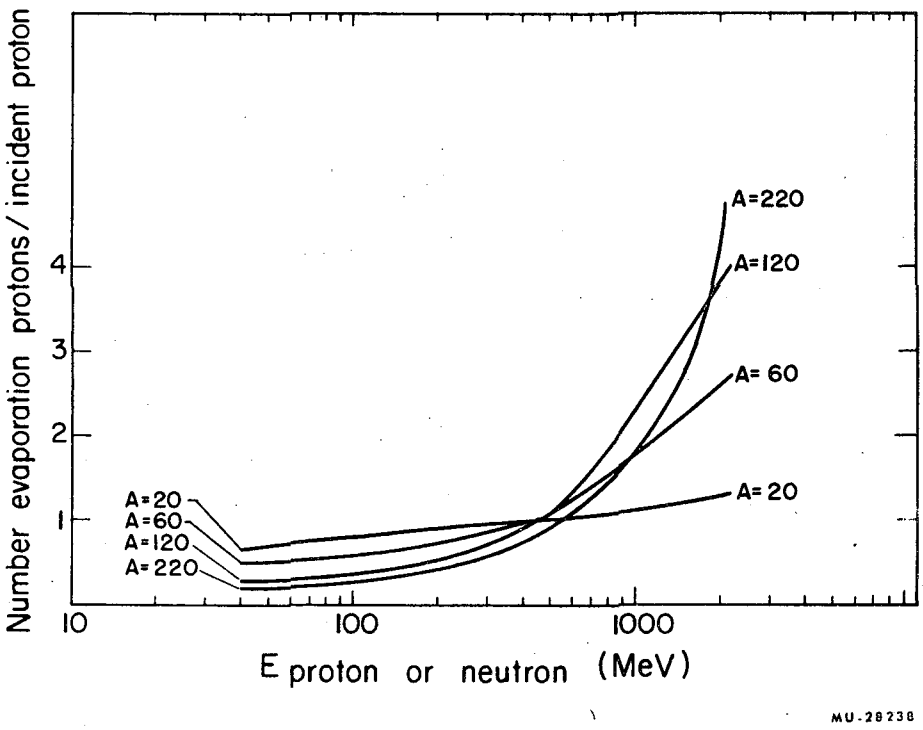
Number evaporation protons / incident proton
4
3
2
1
10
100
1000
E proton or neutron (MeV)
A=220
A=120
A= 60
A= 20
A=20
A=60
A=120
A=220
MU-28238

Fig. 16.

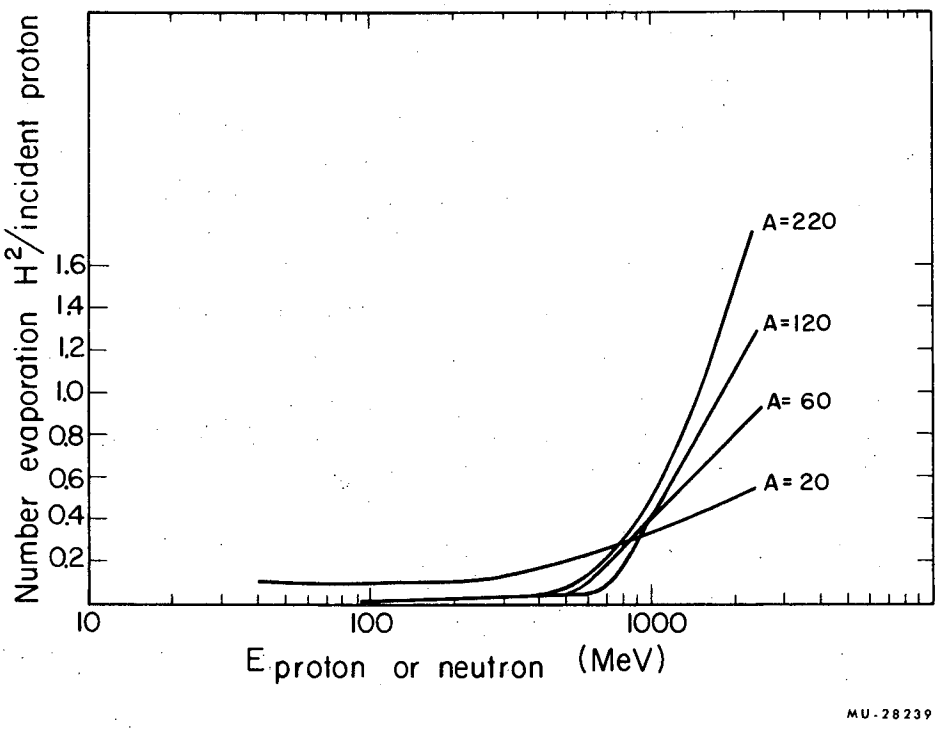
Number evaporation H²/incident proton
1.6
1.4
1.2
1.0
0.8
0.6
0.4
0.2
10
100
1000
E proton or neutron (MeV)
A=220
A=120
A= 60
A= 20
MU-28239

Fig. 17.

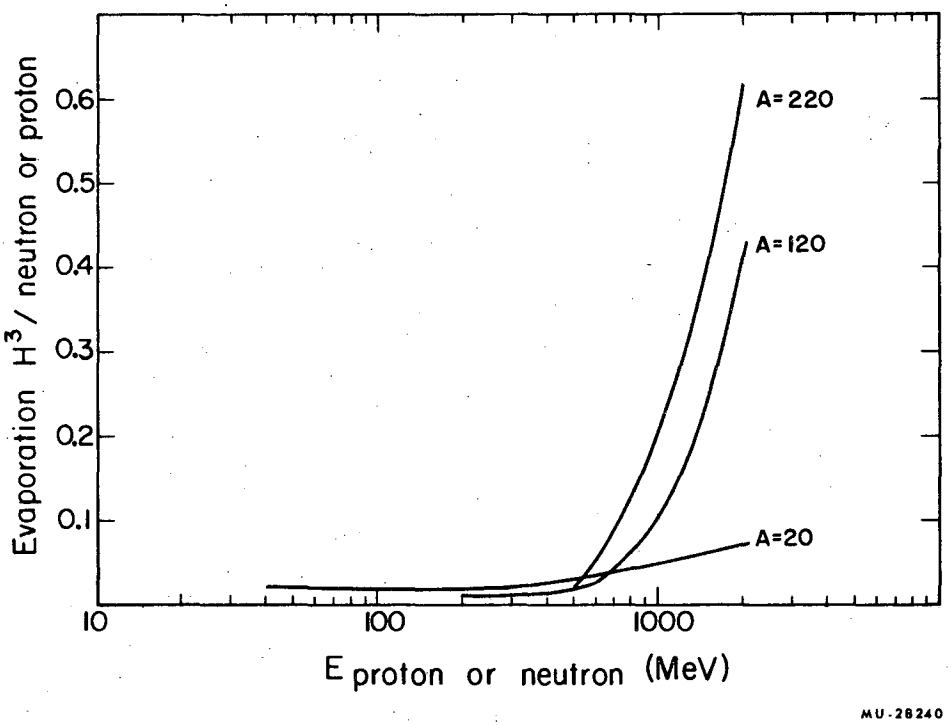
Evaporation H^3 / neutron or proton
0.6
0.5
0.4
0.3
0.2
0.1
A=220
A=120
A=20
10
100
1000
E proton or neutron (MeV)
MU-28240

Fig. 18.

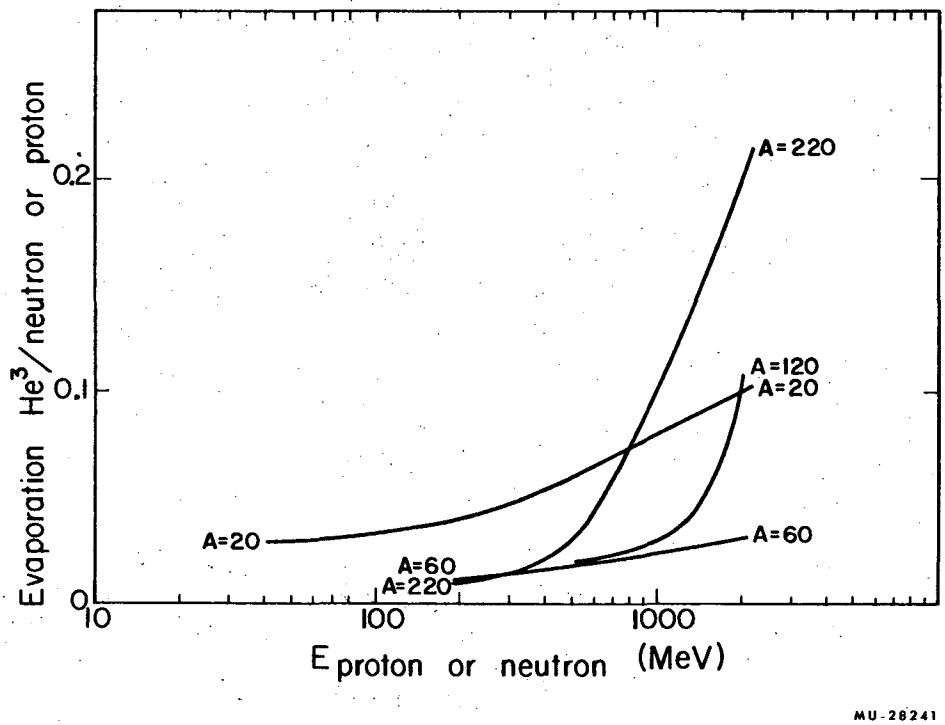
Evaporation He^3/neutron or proton
0.2
0.1
0
10
100
1000
E proton or neutron (MeV)
A=220
A=120
A=20
A=20
A=60
A=60
A=220
MU-28241

Fig. 19.

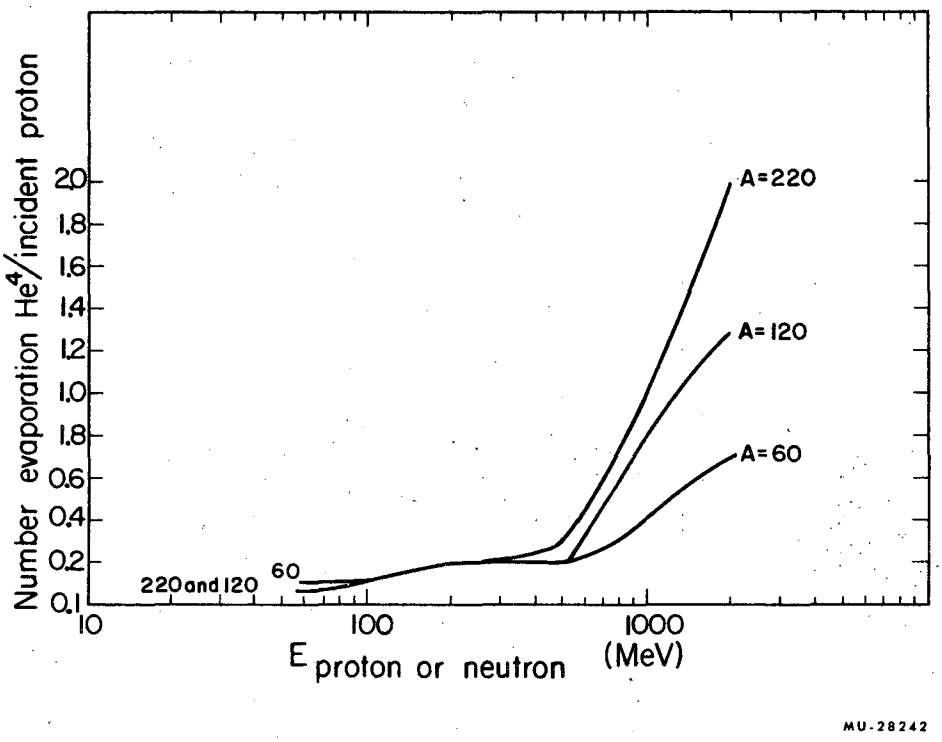
Number evaporation He4/incident proton
2.0
1.8
1.6
1.4
1.2
1.0
1.8
0.6
0.4
0.2
0.1
10
100
1000
E proton or neutron (MeV)
A=220
A=120
A=60
220 and 120
60
MU-28242

Fig. 20.

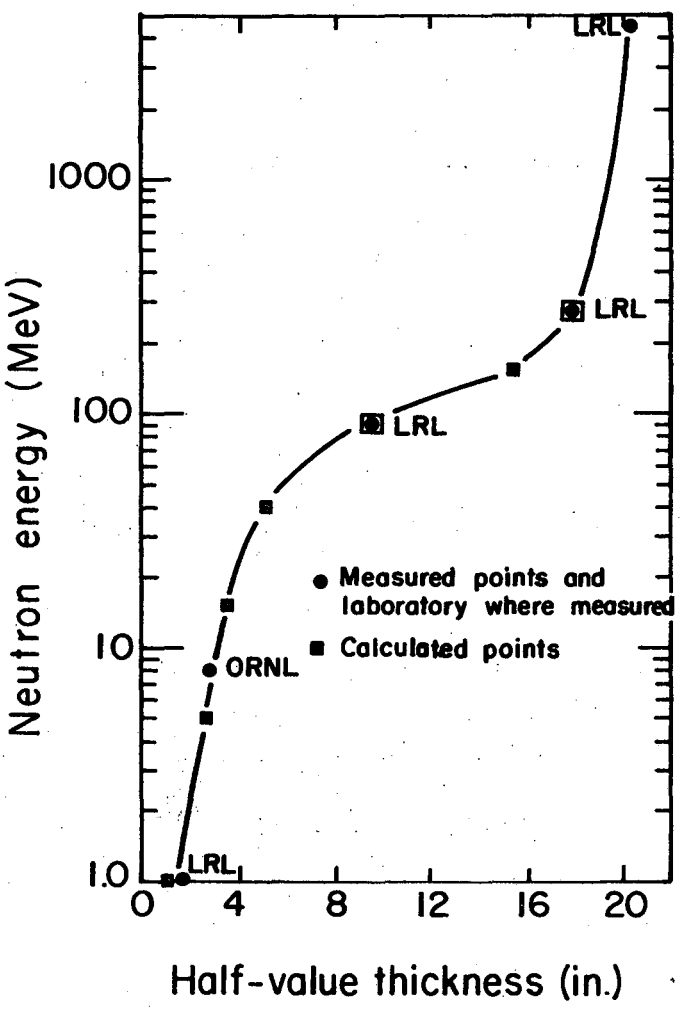
Neutron energy (MeV)
1000
100
10
1.0
0
4
8
12
16
20
Half-value thickness (in.)
LRL
LRL
LRL
ORNL
LRL
● Measured points and laboratory where measured
■ Calculated points
MU-26629

Fig. 21.